



Potential energy surfaces for the $\text{HBr}^+ + \text{CO}_2 \rightarrow \text{Br} + \text{HOCO}^+$ reaction in the HBr^+ $2\Pi_{3/2}$ and $2\Pi_{1/2}$ spin-orbit states

Rui Sun, Giovanni Granucci, Amit K. Paul, Matthew Siebert, Hongliang J. Liang, Grace Cheong, William L. Hase, and Maurizio Persico

Citation: *The Journal of Chemical Physics* **142**, 104302 (2015); doi: 10.1063/1.4913767

View online: <http://dx.doi.org/10.1063/1.4913767>

View Table of Contents: <http://scitation.aip.org/content/aip/journal/jcp/142/10?ver=pdfcov>

Published by the [AIP Publishing](#)

Articles you may be interested in

Accurate ab initio potential energy surface, thermochemistry, and dynamics of the $\text{Br}(2P, 2P_{3/2}) + \text{CH}_4 \rightarrow \text{HBr} + \text{CH}_3$ reaction

J. Chem. Phys. **138**, 134301 (2013); 10.1063/1.4797467

Communication: A chemically accurate global potential energy surface for the $\text{HO} + \text{CO} \rightarrow \text{H} + \text{CO}_2$ reaction

J. Chem. Phys. **136**, 041103 (2012); 10.1063/1.3680256

Rotational dependence of the proton-transfer reaction $\text{HBr}^+ + \text{CO}_2 \rightarrow \text{HOCO}^+ + \text{Br}$. II. Comparison of HBr^+ ($2\Pi_{3/2}$) and HBr^+ ($2\Pi_{1/2}$)

J. Chem. Phys. **133**, 234301 (2010); 10.1063/1.3515300

Theoretical mechanistic study on the ion-molecule reactions of $\text{CCN}^+ / \text{CNC}^+$ with H_2O and $\text{HCO}^+ / \text{HOC}^+$ with HCN/HNC




J. Chem. Phys. **116**, 1892 (2002); 10.1063/1.1431272

State-specific reactions $\text{HBr} + (2\Pi_{i,v}) + (\text{H}_2, \text{HBr}) \rightarrow \text{H}_2\text{Br} +$ at low collisional energies

J. Chem. Phys. **114**, 6625 (2001); 10.1063/1.1355661

AIP | The Journal of
Chemical Physics

Meet The New Deputy Editors

 Peter Hamm	 David E. Manolopoulos	 James L. Skinner
---	--	---

Potential energy surfaces for the $\text{HBr}^+ + \text{CO}_2 \rightarrow \text{Br} + \text{HOCO}^+$ reaction in the $\text{HBr}^+ \ ^2\Pi_{3/2}$ and $\ ^2\Pi_{1/2}$ spin-orbit states

Rui Sun,¹ Giovanni Granucci,² Amit K. Paul,¹ Matthew Siebert,^{1,3} Hongliang J. Liang,⁴ Grace Cheong,⁵ William L. Hase,¹ and Maurizio Persico²

¹Department of Chemistry and Biochemistry, Texas Tech University, Lubbock, Texas 79409, USA

²Dipartimento di Chimica e Chimica Industriale, University of Pisa, Pisa, Italy

³Department of Chemistry, Missouri State University, Springfield, Missouri 65879, USA

⁴Department of Engineering, Swarthmore College, Swarthmore, Pennsylvania 19081, USA

⁵Department of Chemistry, Haverford College, Haverford, Pennsylvania 19041, USA

(Received 31 December 2014; accepted 17 February 2015; published online 9 March 2015)

Quantum mechanical (QM) + molecular mechanics (MM) models are developed to represent potential energy surfaces (PESs) for the $\text{HBr}^+ + \text{CO}_2 \rightarrow \text{Br} + \text{HOCO}^+$ reaction with HBr^+ in the $\ ^2\Pi_{3/2}$ and $\ ^2\Pi_{1/2}$ spin-orbit states. The QM component is the spin-free PES and spin-orbit coupling for each state is represented by a MM-like analytic potential fit to spin-orbit electronic structure calculations. Coupled-cluster single double and perturbative triple excitation (CCSD(T)) calculations are performed to obtain “benchmark” reaction energies without spin-orbit coupling. With zero-point energies removed, the “experimental” reaction energy is 44 ± 5 meV for $\text{HBr}^+(\ ^2\Pi_{3/2}) + \text{CO}_2 \rightarrow \text{Br}(\ ^2P_{3/2}) + \text{HOCO}^+$, while the CCSD(T) value with spin-orbit effects included is 87 meV. Electronic structure calculations were performed to determine properties of the BrHOCO^+ reaction intermediate and $[\text{HBr} \cdots \text{OCO}]^+$ van der Waals intermediate. The results of different electronic structure methods were compared with those obtained with CCSD(T), and UMP2/cc-pVTZ/PP was found to be a practical and accurate QM method to use in QM/MM direct dynamics simulations. The spin-orbit coupling calculations show that the spin-free QM PES gives a quite good representation of the shape of the PES originated by $\ ^2\Pi_{3/2}\text{HBr}^+$. This is also the case for the reactant region of the PES for $\ ^2\Pi_{1/2}\text{HBr}^+$, but spin-orbit coupling effects are important for the exit-channel region of this PES. A MM model was developed to represent these effects, which were combined with the spin-free QM PES. © 2015 AIP Publishing LLC. [<http://dx.doi.org/10.1063/1.4913767>]

I. INTRODUCTION

There is considerable experimental interest in the chemical dynamics of ion-molecule reactions with the reactants in specific quantum states.^{1–7} Viggiano and co-workers¹ have investigated the influence of vibrational and rotational energies on the rates of ion-molecule reactions. For exothermic reactions, they found that rotational energy has a negligible influence on the reaction efficiency, while rotational energy increases the efficiency for endothermic reactions. More detailed information regarding the role of different types of energy on the reaction dynamics is obtained by studying state-selected molecular ions.² Anderson and co-workers^{3–5} have been particularly interested in the effects of reactant vibrational excitation on the dynamics of ion-molecule reactions.

In recent research, Paetow *et al.*^{6,7} used a guided ion beam apparatus to measure the rate constants for HBr^+ and DBr^+ , in the $\ ^2\Pi_{3/2}$ and $\ ^2\Pi_{1/2}$ spin-orbit (SO) states, reacting with CO_2 to form $\text{Br} + \text{HOCO}^+/\text{DOCO}^+$. The mean rotational energy of the HBr^+ and DBr^+ ions was varied and it was found that the rate constant decreased with increase in rotational energy. Similarly, the rate constants decreased with increase in reactant collision energy. These energy and state specific effects were found for both the endothermic reaction with $\text{HBr}^+(\text{DBr}^+)$ in the $\ ^2\Pi_{3/2}$ state and the exothermic reaction with these ions in

the $\ ^2\Pi_{1/2}$ state. The potential energy surface (PES) for these proton and deuteron transfer reactions has been investigated at the UMP2 and coupled-cluster single double and perturbative triple excitation (CCSD(T)) levels of theory,^{6,8} without the inclusion of SO coupling,⁹ and the resulting energies are summarized in Table I. An important feature of the PES is the reaction intermediate BrHOCO^+ (BrDOCO^+). The 0 K experimental reaction energetics^{10,11} are depicted in Figure 1.

Classical trajectory simulations have proven very important for interpreting experimental studies of state-selected ion-molecule reactions and determining atomistic details of their chemical dynamics. Of particular interest is the manner in which vibrational excitation of the reactants may enhance the reaction rate, which has been investigated for the reaction of H_2CO^+ with D_2 and CD_4 ,^{13,14} and the $\text{NO}_2^+ + \text{C}_2\text{H}_2$, and $\text{C}_2\text{H}_2^+ + \text{CH}_4$ reactions.^{15,16} The possibility of establishing of “Polanyi Rules” for polyatomic reactions has been investigated.¹³ Trajectories have also been used to investigate the role of state-specific vibrational excitation on collision-induced dissociation.¹⁷

In the work reported here, SO coupling calculations⁹ are performed to derive PESs for the $\text{HBr}^+ + \text{CO}_2 \rightarrow \text{Br} + \text{HOCO}^+$ reaction with HBr^+ in the $\ ^2\Pi_{3/2}$ and $\ ^2\Pi_{1/2}$ spin-orbit states, which in the following are denoted as $\ ^2\Pi_{3/2}$ PES and $\ ^2\Pi_{1/2}$ PES. An electronic structure quantum mechanical (QM)

TABLE I. CCSD(T) and UMP2 energies for the $\text{HBr}^+ + \text{CO}_2 \rightarrow \text{Br} + \text{HOCO}^+$ reaction.^a

Theory	$E^{\text{QM}}(\text{BrHOCO}^+)$	ΔE_r^{QM}
UMP2/DZP ^b	-706(-580)	-132(25)
UMP2/TZ2P ^c	-840(-729)	-114(41)
CCSD(T)/TZ2P ^b		-135(27)
CCSD(T)//PMP2/TZ2P ^b	-824(-713)	-133(22)
CCSD(T)/cc-pVTZ/SDB		-42
CCSD(T)/cc-pVQZ/SDB		-6
CCSD(T)/aug-cc-pVTZ/SDB		86
CCSD(T)/aug-cc-pVQZ/SDB		77
CCSD(T)/cc-pVDZ/PP	-668	16
CCSD(T)/cc-pVTZ/PP	-698	67
CCSD(T)/cc-pVQZ/PP		73
CCSD(T)/CBS/cc-pVXZ/PP		75
CCSD(T)/aug-cc-pVDZ/PP		152
CCSD(T)/aug-cc-pVTZ/PP		161
CCSD(T)/aug-cc-pVQZ/PP		102
CCSD(T)/CBS/aug-cc-pVXZ/PP		62

^aEnergies are in meV and are with respect to zero of energy for $\text{HBr}^+ + \text{CO}_2$. Zero-point energies are not included in $E^{\text{QM}}(\text{BrHOCO}^+)$, the energy of the BrHOCO^+ intermediate with respect to reactants, and ΔE_r^{QM} , the reaction energy. Harmonic zero-point corrected energy are included in parenthesis.

^bFor Br, a SDD pseudopotential and a valence basis set of double zeta quality were used; from Refs. 7 and 8.

^cFor Br, a SDB pseudopotential and a valence basis set of cc-pVTZ quality were used; from Refs. 7 and 8.

theory is used to represent the “average” $^2\Pi$ PES without spin-orbit coupling. Analytic molecular mechanics (MM)-like potential energy functions, which are fit to the spin-orbit coupling calculations, are then added to this QM component to give QM + MM¹⁸ PESs with spin-orbit coupling. These potential energy surfaces may be used in future QM + MM direct dynamics simulations¹⁸ to study the $\text{HBr}^+ + \text{CO}_2 \rightarrow \text{Br} + \text{HOCO}^+$ reaction with HBr^+ in the $^2\Pi_{3/2}$ and $^2\Pi_{1/2}$ spin-orbit states. The reason for resorting to an analytic representation

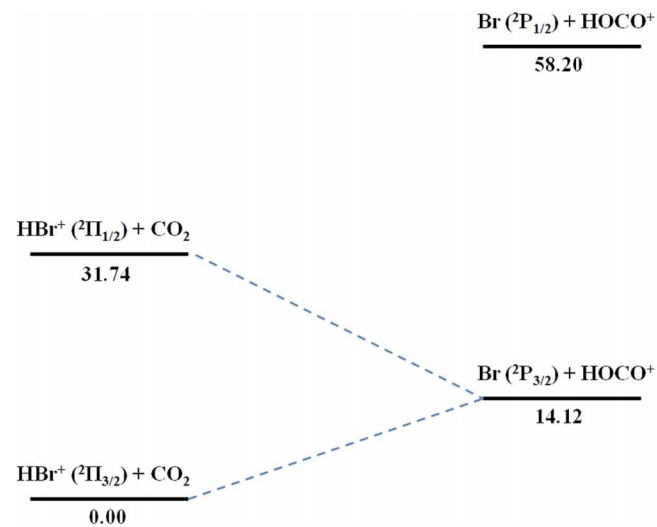


FIG. 1. Experimental energies^{10,11} (in kJ/mol) for the proton-transfer reactions of CO_2 with $\text{HBr}^+(^2\Pi_{3/2})$ and $\text{HBr}^+(^2\Pi_{1/2})$, respectively. The temperature is 0 K and ZPEs are included. The excitation energy from $\text{HBr}^+(^2\Pi_{3/2})$ to $\text{HBr}^+(^2\Pi_{1/2})$ is from Ref. 12.

of the spin-orbit contribution to the PES is that different electronic structure methods are best suited for the spin-free and for the spin-orbit calculations, which would make the direct evaluation of the spin-orbit effect quite expensive. Moreover, most electronic structure packages cannot compute analytic gradients for the spin-orbit corrected PESs, as needed in direct dynamics simulations.^{19,20}

II. COMPUTATIONAL METHODS

Without SO coupling HBr^+ has a four-fold degenerate $^2\Pi$ state. With SO coupling, this state splits into a doubly degenerate $^2\Pi_{3/2}$ SO ground state and a doubly degenerate $^2\Pi_{1/2}$ SO state which is 329 meV higher in energy.^{12,21} Also considered for the SO coupling calculations described below is the HBr^+ doubly degenerate $^2\Sigma_{1/2}$ state. The $^2P_{3/2}$ ground electronic state of the Br atom is four-fold degenerate, and both the $^2\Pi_{3/2}$ and $^2\Pi_{1/2}$ states of the HBr^+ reactant correlate with this product $^2P_{3/2}$ state. The $^2\Sigma_{1/2}$ state of HBr^+ correlates with the doubly degenerate $^2P_{1/2}$ excited state of the Br atom. The $^2P_{3/2}$ and $^2P_{1/2}$ states of Br are separated by 457 meV. In a $\text{BrH}^+ \cdots \text{OCO}$ collinear arrangement and without SO coupling, the ground electronic state remains $^2\Pi$ as for the reactants and is four-fold degenerate. For bent planar geometries, these degenerate states split into a $^2A''$ term and a $^2A'$ term, still very close in energy.

A. Calculations without spin-orbit coupling

In previous work, MP2 and CCSD(T) electronic structure calculations were performed, without SO coupling, for the $\text{HBr}^+ + \text{CO}_2 \rightarrow \text{HOCO}^+ + \text{Br } ^2A''$ ground state PES.^{6,8} For the work reported here, these calculations were supplemented with additional electronic structure calculations performed with the NWChem computer program.²²

CCSD(T)²³ calculations, with both augmented and non-augmented correlation consistent double, triple, and quadruple zeta basis sets,²⁴ were used to calculate the $\text{HBr}^+ + \text{CO}_2 \rightarrow \text{HOCO}^+ + \text{Br } ^2A''$ heat of reaction without SO coupling. The complete basis set (CBS) limit for these calculations was obtained using the formula of Peterson *et al.*,^{25,26} i.e.,

$$E(n) = E_{\text{CBS}} + A \exp[-(n-1)] + B \exp[-(n-1)^2], \quad (1)$$

where $n = 2, 3$, and 4, represent $X = \text{D, T, and Q}$, respectively, for the cc-pVXZ basis sets.

A large number of basis functions are needed to accurately describe all the electrons for heavy atoms with many electrons, and the size of the basis set becomes important in treating both scalar and spin-orbit relativistic effects. Since the core electrons do not play an important role in chemical reactions, methods have been developed^{27,28} to replace the core electrons by effective core potentials (ECPs) or pseudopotentials (PPs).²⁹⁻³¹ In the research presented here, the energy-consistent Stuttgart-Dresden-Bonn (SDB)³² PP and small-core PPs³³ were used for the many electron Br atom for both accuracy and efficiency.

To compare with the benchmark CCSD(T)/CBS calculations, the reaction potential energy profile was also calculated

with the three widely used density functional theory (DFT) functionals B3LYP,³⁴ PBE0,³⁵ and Becke98,³⁶ and unrestricted MP2.³⁷ A variety of basis sets were used for these calculations with the goal of ascertaining whether the reaction potential energy profile may be accurately represented by a single reference method with low computational cost.

For a collinear geometry, the ground state for the $\text{HBr}^+ + \text{CO}_2 \rightarrow \text{HOCO}^+ + \text{Br}$ reaction is identified as ${}^2\Pi$, which splits into ${}^2A''$ and ${}^2A'$ levels for bent planar geometries at which the interaction between the Br atom and CO_2 is not negligible. To study this splitting, two distinct ROHF calculations were performed followed by MP2 calculations. These ROHF-MP2 calculations for the ${}^2A'$ state had occupation $\dots(21a')^2(7a'')^2(22a')^1$ and for the ${}^2A''$ state had occupation $\dots(21a')^2(7a'')^1(22a')^2$.

B. Anharmonic zero-point energy corrections without spin-orbit coupling

The experimental heats of formation for the reactants and products are CO_2 , -393.107 ± 0.014 kJ/mol; HBr^+ , 1097.71 ± 0.14 kJ/mol; HOCO^+ , 600.80 ± 0.45 kJ/mol; and Br, 117.92 ± 0.06 kJ/mol.³⁸ The resulting 0 K $\Delta H = \Delta E$ for the $\text{HBr}^+({}^2\Pi_{3/2}) + \text{CO}_2 \rightarrow \text{HOCO}^+ + \text{Br}({}^2P_{3/2})$ reaction is 14.12 ± 0.47 kJ/mol (146 ± 5 meV). To compare with the *ab initio* reaction energetics, an experimental value for $\Delta H = \Delta E$ is required which does not include zero-point energies (ZPEs) for the reactants and products. The following procedures were used to remove ZPE from the experimental 0 K heat of reaction.

To second-order³⁹ and also for the Morse potential function,⁴⁰ the vibrational energy levels for a diatomic molecule are given by

$$E(n) = \left(n + \frac{1}{2}\right) h\nu_e + \left(n + \frac{1}{2}\right)^2 h x_e, \quad (2)$$

where ν_e is the harmonic frequency and x_e is the anharmonic correction term. These parameters are known for HBr^+ and are $\nu_e = 2441.5$ cm^{-1} and $x_e = 47.4$.⁴¹ The HBr^+ ZPE is $(h\nu_e/2 - hx_e/4) = 14.74$ kJ/mol.

The vibrational energy levels for CO_2 , given by second-order perturbation theory,³⁹ are

$$E(n, d) = \sum_{i=1}^3 \left(n_i + \frac{d_i}{2}\right) h\nu_{i,e} + \sum_{i=1}^3 \sum_{k \geq i}^3 \left(n_i + \frac{d_i}{2}\right) \times \left(n_k + \frac{d_k}{2}\right) h x_{i,k} + h g_{22} l^2, \quad (3)$$

which is similar to Eq. (2) with the additional parameters d the degeneracy of the vibrational levels, g_{22} the vibrational angular momentum anharmonicity constant, and l the vibrational angular momentum. The parameters for the CO_2 vibrational energy levels are (all in cm^{-1}):³⁹ $\nu_{1,e} = 1354.0$, $\nu_{2,e} = 673.2$, $\nu_{3,e} = 2396.3$, $x_{11} = -2.9$, $x_{22} = +1.1$, $x_{33} = -12.5$, $x_{12} = -3.6$, $x_{13} = -19.7$, $x_{23} = -12.4$, and $g_{22} = -0.9$. For the ZPE level, the n_i and l are zero, so that the CO_2 ZPE is 30.33 kJ/mol.

The vibrational energy levels for the product molecule HOCO^+ have not been measured, and thus, experimental

values may not be used to determine the ZPE for this molecule. Therefore, a well-tested electronic structure theory approach, with a scale factor for the anharmonic ZPE,^{42–46} was used. The specific method used is CCSD(T)/cc-pVTZ and the same optimized scale factor for each mode, determined by a least-squares minimization of the residuals between the scaled and experimental ZPEs for a chosen molecular database. The resulting ZPE for HOCO^+ is 54.95 kJ/mol. This approach was also used to determine the ZPE for the BrHOCO^+ reaction intermediate considered in Sec. III.

With the above values for the HBr^+ , CO_2 , and HOCO^+ ZPEs, the 14.12 ± 0.47 kJ/mol (146 ± 5 meV) heat of reaction at 0 K becomes 4.24 ± 0.47 kJ/mol (44 ± 5 meV) without ZPEs. These are energies for the ground-state $\text{HBr}^+({}^2\Pi_{3/2}) + \text{CO}_2 \rightarrow \text{Br}({}^2P_{3/2}) + \text{HOCO}^+$ pathway. Furthermore, we can assume that the splitting of the ${}^2\Pi$ multiplet of HBr^+ and of the 2P multiplet of Br is only due to the SO interaction of the states belonging to the same multiplets, because other states are well separated in energy. Then, the SO contribution to the ground state energy of HBr^+ is half the splitting, i.e., 164.5 meV,^{12,21} and in the case of Br, it is one third of the splitting, i.e., 152.3 meV.⁴⁷ So, the spin-orbit contribution to the reaction energy is very small, about 12 meV. By subtracting this contribution, we find that the reaction energy without ZPE and without SO is 32 ± 5 meV.

C. Calculations with spin-orbit coupling

The spin-free states for the $\text{HBr}^+ + \text{CO}_2$ reaction are coupled by SO interactions and mix, producing a new set of states identified as ${}^2\Pi_{3/2}$ and ${}^2\Pi_{1/2}$. SO coupling calculations were carried out with the Breit Pauli Hamiltonian, as implemented in the Molpro⁴⁸ program using the state averaged complete active space self-consistent field (SA-CASSCF) theory,⁴⁹ to determine PESs for these ${}^2\Pi_{3/2}$ and ${}^2\Pi_{1/2}$ states. Dunning's cc-pVTZ basis set⁵⁰ was used (fully uncontracted and up to p functions for H, d for C and O, and f for Br). In order to run meaningful SO coupling calculations, three degenerate $4p^5$ states of the Br atom need to be included, which correspond to the ground ${}^2\Pi$ state plus a ${}^2\Sigma$ excited state of HBr^+ . However, if equal weights were applied to the three states to perform a SA-CASSCF calculation, the ${}^2\Sigma$ state would be higher in energy than a charge transfer state, $\text{HBr} + \text{CO}_2^+({}^2\Pi)$. To remove this latter state, we used the "dynamical weighting" ansatz, as implemented in Molpro; i.e., the weight of each state is computed as

$$w_i = 1 / \cosh(\alpha \Delta E_i)^2, \quad (4)$$

where ΔE_i is the energy difference between state i and the ground state. Setting the constant α to 9 a.u. enables the program to shift the charge transfer ${}^2\Pi$ state to a higher energy than the ${}^2\Sigma$ state, so that only 3 states had to be taken into account in the SA-CASSCF calculations. The active space includes 5 orbitals and 9 electrons, which are one σ molecular orbital (MO) and a pair of π non-bonding MO's on HBr, and a pair of π bonding MO's on CO_2 for the reactants; and the three $4p$ orbitals of Br, and one a' MO and one a'' MO on HOCO^+ for the products.

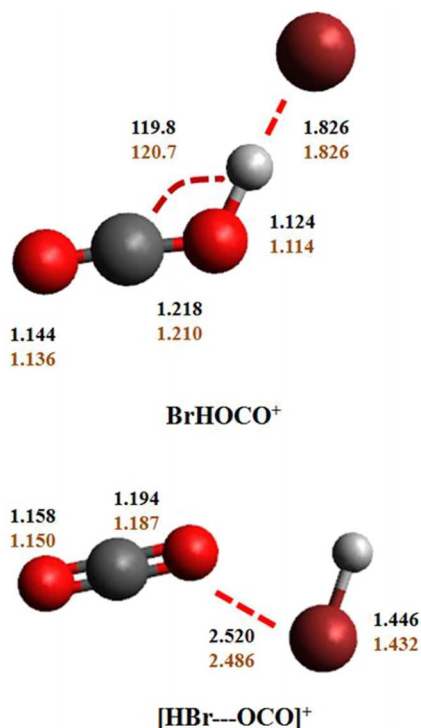


FIG. 2. Geometries of the intermediate BrHOCO^+ and van der Waals complex $[\text{HBr}\cdots\text{OCO}]^+$. The unit of bond length is Angstrom and bond angle is in degrees. The bottom numbers are, respectively, for CCSD(T)/cc-pVDZ/PP and CCSD(T)/cc-pVTZ/PP.

III. COMPUTATIONAL RESULTS

A. PES without spin-orbit coupling

1. CCSD(T) PES

As discussed in the Introduction, a goal of this study is to develop accurate QM+MM PESs¹⁸ for the $\text{HBr}^+ + \text{CO}_2 \rightarrow \text{Br} + \text{HOCO}^+$ reaction with HBr^+ in the $^2\Pi_{1/2}$ and $^2\Pi_{3/2}$ spin-orbit states. In this model, QM represents the average $^2\Pi$ PES without spin-orbit coupling and MM are analytic potential energy functions fit to spin-orbit coupling calculations (see below). An accurate QM model is required for this representation of the PES. As for other QM+MM models,^{18,51–53} the terms for each PES are additive with one QM and the other MM.

In previous work,⁷ Paetow *et al.* calculated QM energies for the $\text{HBr}^+ + \text{CO}_2 \rightarrow \text{Br} + \text{HOCO}^+$ reaction with UMP2 and CCSD(T) theories and double- and triple-zeta basis sets. Values for the reaction energy, ΔE_r , and the energy of the reaction intermediate BrHOCO^+ , $E(\text{BrHOCO}^+)$, were reported without ZPEs included and with a harmonic ZPE correction. As shown in Table I, the calculated ΔE_r^{QM} , without a ZPE correction range from approximately -114 to -135 meV.

a. $\text{HBr}^+ + \text{CO}_2 \rightarrow \text{Br} + \text{HOCO}^+$ reaction energy. With the objective to establish an accurate QM energy for the $\text{HBr}^+ + \text{CO}_2 \rightarrow \text{Br} + \text{HOCO}^+$ reaction, a set of CCSD(T) calculations were performed to determine the reaction energy ΔE_r . Two pseudo potentials were considered for Br, i.e., PP by Peterson *et al.*⁵⁴ and SDB by Martin and Sundermann.⁵⁵ In addition, a range of different correlation consistent cc-pVXZ and aug-cc-pVXZ basis sets⁵⁰ were used, with $X = \text{D, T, and}$

TABLE II. Comparison of CCSD(T), UMP2, and DFT reaction energies.^{a,b}

Basis set	Method			
	B3LYP	B98	PBE0	UMP2
	ΔE_r^{QM}			
3-21G				-477
6-31G**/lanl2dz	-460			
6-31G**/lanl2dzdp	-154	-144	-156	
6-311G				-197
6-311G**	6	-5	13	5
6-311G**/SDB				-199
cc-pVDZ/PP	-31(64)	-37	-11	-30
cc-pVTZ/PP				83
cc-pVTZ/SDB	10(125)	-24	-24	-43
aug-cc-pVDZ/lanl2dzdp	102(216)	81	71	309
aug-cc-pVTZ/SDB	104(218)	79	75	83
	$E^{\text{QM}}(\text{BrHOCO}^+)$			
3-21G				-635
6-31G**/lanl2dz	-1111			
6-31G**/lanl2dzdp	-898	-898	-931	
6-311G				
6-311G**	-792	-816	-831	
6-311G**/SDB				-865
cc-pVDZ/PP	-868	-875	-878	-739
cc-pVTZ/PP				-731
cc-pVTZ/SDB	-809(-753)	-847	-878	-811
aug-cc-pVDZ/lanl2dzdp	-731(-692)	-762	-798	
aug-cc-pVTZ/SDB	-741(-699)	-781	-815	-779

^aEnergies are in meV and are with respect to zero of energy for $\text{HBr}^+ + \text{CO}_2$. Zero-point energies are not included in $E^{\text{QM}}(\text{BrHOCO}^+)$, the energy of the BrHOCO^+ intermediate with respect to reactants, and ΔE_r^{QM} , the reaction energy. Harmonic zero-point energy corrections are included for the energies in parenthesis.

^bAs benchmark results to compare with, ΔE_r^{QM} from CCSD(T)/CBS/cc-pVXZ ($X = \text{D, T, Q}$) and CCSD(T)/CBS/aug-cc-pVXZ ($X = \text{D, T, Q}$) are 75 and 62 meV, respectively. $E^{\text{QM}}(\text{BrHOCO}^+)$ from CCSD(T)/CBS/cc-pVXZ ($X = \text{D, T}$) is -710 meV.

Q to represent double-, triple-, and quadruple zeta basis sets, respectively.

The results of these CCSD(T) calculations are listed in Table I. A similar CBS limit is found for the “cc-” and “aug-cc-” basis sets with the PP. For the former basis sets, the CBS limit for the reaction energy ΔE_r^{QM} is 75 meV, while 62 meV for the latter. For the calculations with the SDB pseudopotential, the aug-cc-pVTZ and aug-cc-pVQZ basis sets give ΔE_r^{QM} of 86 and 77 meV, respectively. A comparison of these results, with consideration of effects of the basis set on ΔE_r and also the CBS limit, suggests that the CCSD(T)/CBS/cc-pVXZ/PP value for ΔE_r^{QM} of 75 meV is the most accurate. For these calculations, the cc-pVTZ/PP and cc-pVQZ/PP basis sets give very similar ΔE_r^{QM} values, which are nearly identical to the CBS value. A value of 75 meV is used as the QM benchmark for the reaction energy. This value is only slightly higher than the above “experimental value” of 32 ± 5 meV, obtained by subtracting the ZPE and SO contributions.

Though complete spin-orbit calculations are given below, it is possible to obtain a meaningful approximate ΔE_r value for $\text{HBr}^+(^2\Pi_{3/2}) + \text{CO}_2 \rightarrow \text{Br}(^2P_{3/2}) + \text{HOCO}^+$, *in lieu* of these

Entrance Channel Scans

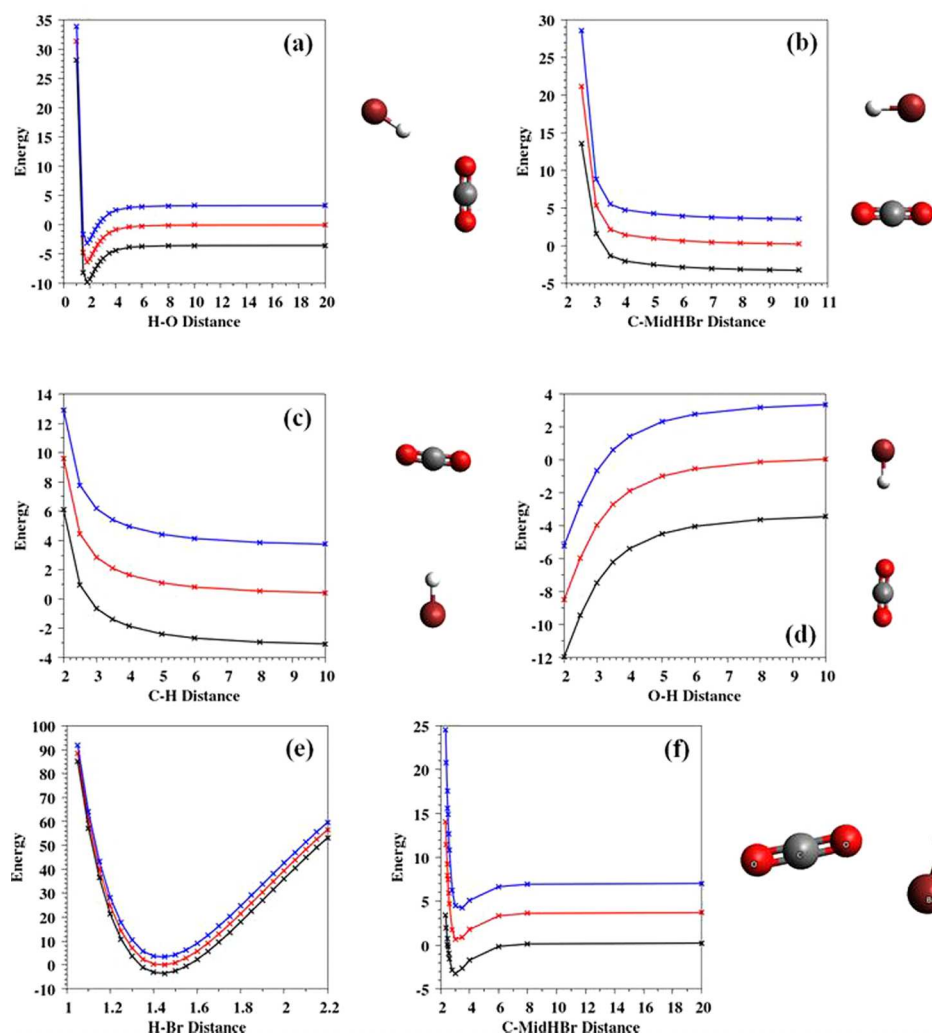


FIG. 3. Representative potential energy (kcal/mol) scans with distance in Å for the $\text{HBr}^+ + \text{CO}_2$ entrance-channel region of the PES. The red, blue, and black lines/dots are, respectively, for the spin free potential energy curve and the curves for the $\text{HBr}^+ \ ^2\Pi_{1/2}$ and $\ ^2\Pi_{3/2}$ states. (a) CO_2 and HBr^+ are fixed at their optimized structures, with H approaching O for a 120° fixed O-H-C angle; (b)-(d) same as (a), except HBr^+ approaches CO_2 with different orientations, and for (c), the O-C-H angle is 89° ; (e) stretching the H-Br $^+$ bond with HBr^+ kept far away from CO_2 (50 Å); and (f) approach of HBr^+ and CO_2 to form the van der Waals complex.

calculations, based on $\Delta E_r^{\text{QM}} = 75$ meV. The splitting of the $\ ^2P_{1/2}$ and $\ ^2P_{3/2}$ state for the Br-atom is 456.9 meV. Since the $\ ^2P_{3/2}$ state is four-fold degenerate and the $\ ^2P_{1/2}$ state is two-fold degenerate, the QM energy for the Br-atom lies 152.3 meV above the $\ ^2P_{3/2}$ energy.⁴⁷ As discussed below as part of the spin-orbit calculations, to a quite good approximation, the QM energy for HBr^+ lies midway between the energies of the $\ ^2\Pi_{1/2}$ and $\ ^2\Pi_{3/2}$ states, each doubly degenerate. The splitting of these two states is 329 meV, placing the QM energy for $\text{HBr}^+ \sim 164.5$ meV above the $\ ^2\Pi_{3/2}$ state.^{12,21} With these QM energies for the Br atom and HBr^+ , and the above value for ΔE_r^{QM} , ΔE_r for the $\text{HBr}^+(\ ^2\Pi_{3/2}) + \text{CO}_2 \rightarrow \text{Br}(\ ^2P_{3/2}) + \text{HOCO}^+$ reaction without ZPE is $(75 - 152.3 + 164.5)$ meV = 87 meV. This value is only slightly higher than the above “experimental value” of 44 ± 5 meV without ZPE, further corrected to 32 ± 5 meV by subtracting the SO contribution.

b. Energies of the BrHOCO^+ and $[\text{HBr} \cdots \text{OCO}]^+$ intermediates. Electronic structure calculations were also performed to determine the QM energy, without ZPE, for the BrHOCO^+ reaction intermediate and the results are given in Table I. The BrHOCO^+ energy, obtained previously by Paetow *et al.*,⁶ from UMP2 and CCSD(T) calculations, varies from -706 to -824 meV, with respect to the separated

reactants $\text{HBr}^+ + \text{CO}_2$. For the current study, an optimized BrHOCO^+ geometry and energy were obtained with CCSD(T) calculations employing the cc-pVDZ/PP and cc-pVTZ/PP basis sets, and their respective energies are -668 and -698 meV (see Table I). Because of the extreme memory requirement for CCSD(T)/cc-pVQZ/PP calculations, it was not possible to obtain an optimized BrHOCO^+ structure and concomitant energy at this level of theory. To approximate the CBS limiting energy for BrHOCO^+ , the above cc-pVDZ and cc-pVTZ energies for BrHOCO^+ were extrapolated using the well-known expression^{56,57}

$$E_X = E^\infty + AX^{-3}, \quad (5)$$

in which X is the cardinal number of the basis set. The resulting CBS limit energy for BrHOCO^+ is -710 meV. As a test of this extrapolation method, the reaction energy (ΔE_r^{QM}) calculated using Eq. (5), and only the double and triple zeta basis sets, was compared with that obtained in Sec. II using Eq. (1) and the double, triple, and quadruple basis sets. ΔE_r^{QM} from Eq. (5) is 88 meV and in a quite good agreement with the value of 75 meV obtained from Eq. (1).

In addition to the BrHOCO^+ reaction intermediate, there is an $[\text{HBr} \cdots \text{OCO}]^+$ van der Waals’ intermediate in the entrance channel of the PES, whose geometry is depicted in

Exit Channel Scans

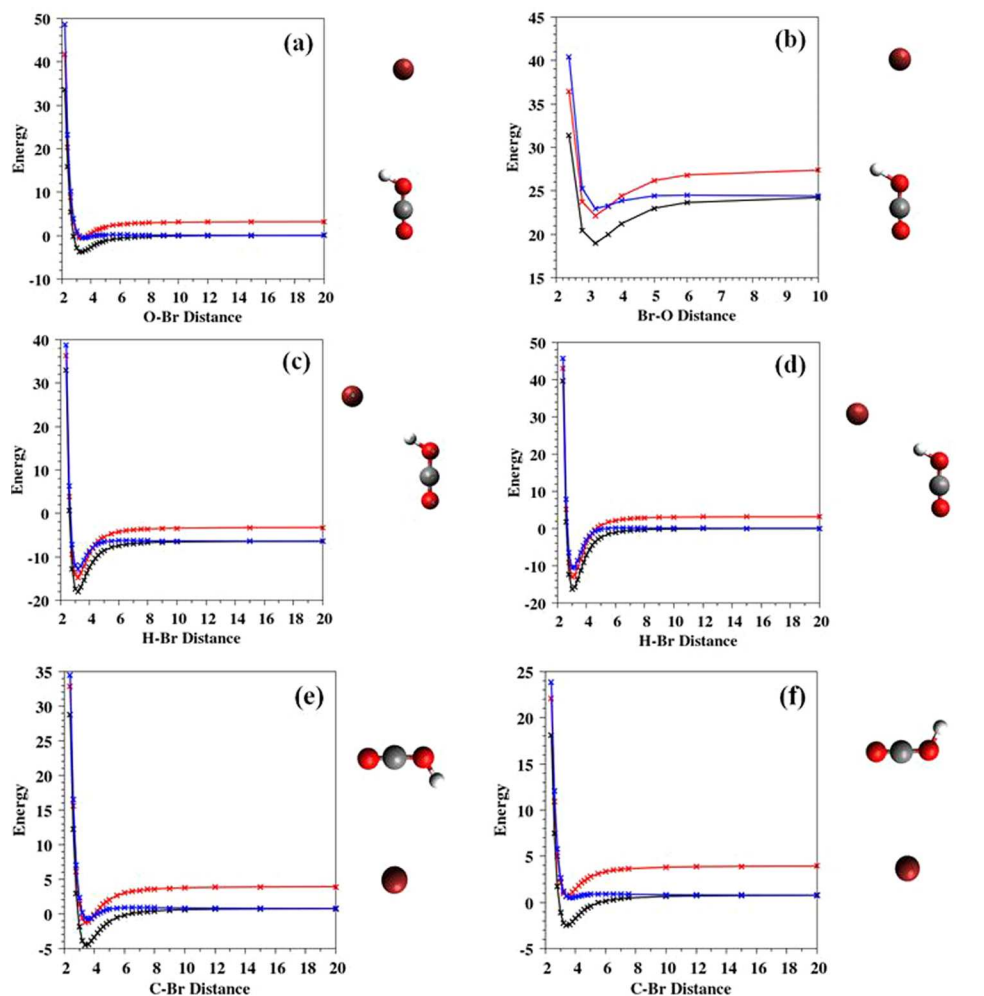


FIG. 4. Representative potential energy (kcal/mol) scans with distance in Å for the Br+HOCO⁺ exit-channel region of the PES. The red, blue, and black lines/dots are, respectively, for the spin free potential energy curve and the curves for the HBr⁺ ²Π_{1/2} and ²Π_{3/2} states. (a) Geometry of HOCO⁺ the same as for the BrHOCO⁺ complex, except the OH bond is stretched to 1.10 Å from the optimized value of 1.00 Å, Br-O-C are collinear; (b) same as (a), except OH bond is stretched to 1.30 Å; and (c) Br approaches HOCO⁺ co-linearly as Br-H-O, with the geometry of HOCO⁺ fixed at that for the BrHOCO⁺ intermediate; (d) same as (c) except OH is stretched to 1.10 Å; (e) and (f) are same as (d) except Br is approaching in different directions.

Figure 2. The CCSD(T) energy for [HBr⋯OCO]⁺, without ZPE, was calculated with the cc-pVDZ and cc-pVTZ basis sets and the respective values are −534 and −539 meV. The CBS extrapolated energy, using Eq. (5), is −541 meV. Thus, the potential energy for the [HBr⋯OCO]⁺ van der Waals' intermediate is ~170 meV higher in energy than that for the BrHOCO⁺ reaction intermediate.

2. An accurate QM method for direct dynamics simulations

As discussed above, CCSD(T) theory, extrapolated to the CBS limit, gives a quite accurate $\Delta E_r^{\text{QM}} = 75$ meV for the HBr⁺ + CO₂ → Br + HOCO⁺ reaction in the absence of spin-orbit coupling. However, this level of theory is impractical for the projected QM+MM direct dynamics simulations and it is important to identify a computationally practical, but sufficiently accurate, QM method for the simulations. Different QM methods and basis sets were tested and the results are summarized in Table II. An ideal QM method would not only give the accurate reaction energy ΔE_r^{QM} but also correctly represent the energies for the intermediates BrHOCO⁺ and [HBr⋯OCO]⁺. In the following, QM energy values are considered for ΔE_r^{QM} , BrHOCO⁺, and [HBr⋯OCO]⁺ consecutively.

Table II shows that Pople-type basis sets give negative or small positive values of ΔE_r^{QM} compared to the CCSD(T)/CBS value of 75 meV. This result was illustrated previously by the calculations of Paetow *et al.*⁶ To illustrate the results in Table II, UMP2/6-311G, UMP2/6-311G*, and PBE0/6-311G* give ΔE_r^{QM} values of −197, 5, and 13 meV, respectively. Accurate values for ΔE_r^{QM} are obtained with the Dunning correlation consistent (cc) basis sets.⁴⁹ B98 and PBE0, with the aug-cc-pVDZ/lanl2dzd basis, give respective ΔE_r^{QM} values of 81 and 71 meV. UMP2 gives $\Delta E_r^{\text{QM}} = 83$ meV with the aug-cc-pVTZ/SDB basis set. The B3LYP ΔE_r^{QM} values with the “cc” basis sets are somewhat larger than the CCSD(T)/CBS value of 75 meV, i.e., with the aug-cc-pVDZ/lanl2dzd and aug-cc-pVDZ/SDB basis sets, the values are 102 and 104 meV, respectively.

The results in Table II show that the calculated energy for the BrHOCO⁺ reaction intermediate strongly depends on the method, basis set, and pseudopotential. DFT and MP2 using Pople-type basis sets and the lanl2dz pseudopotential substantially overestimate the HBr⁺ + CO₂ → BrHOCO⁺ binding energy as compared to the CCSD(T)/CBS(D+T) value of −710 meV. The performance of DFT improves as the basis set gets larger, e.g., the binding energy is ~−790 meV for B3LYP/6-311G**. Of the different DFT functionals, B3LYP with the aug-cc-pVTZ/SDB and aug-cc-pVDZ/lanl2dzd

Exit Channel Scans

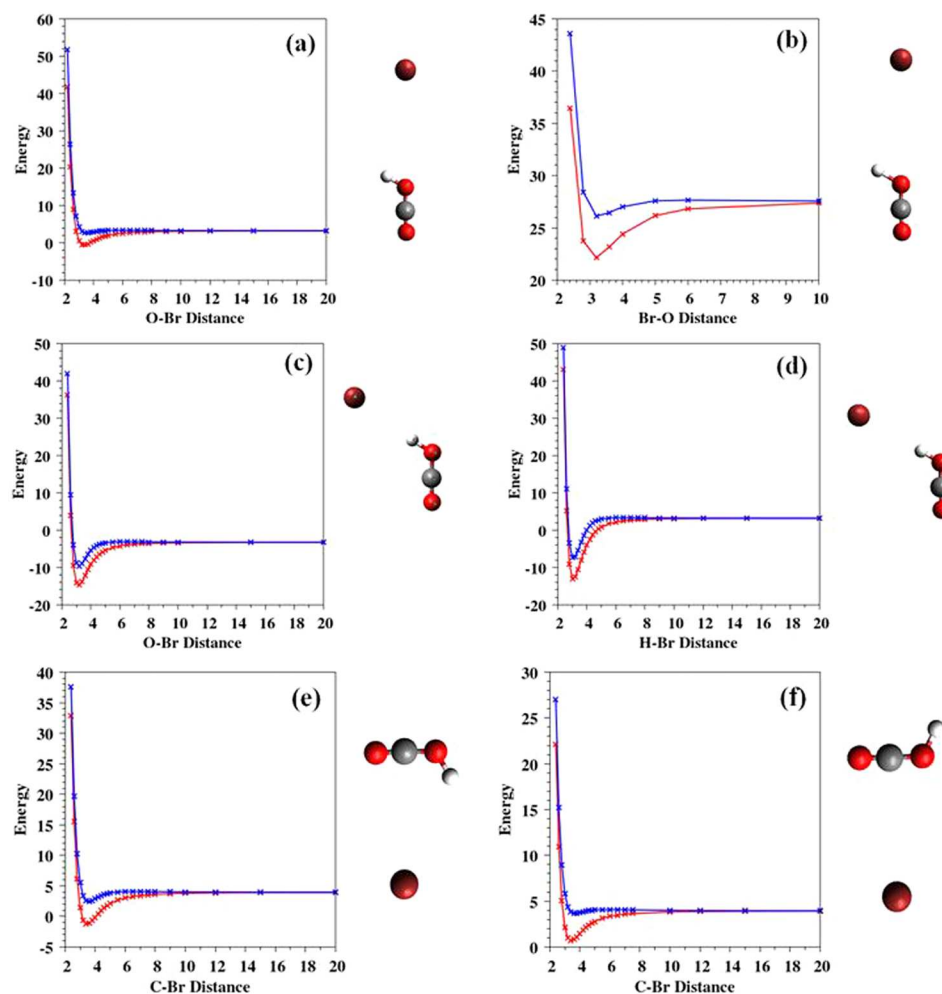


FIG. 5. Potential energy (kcal/mol) scans with distance in Å for the Br + HOCO⁺ entrance-channel region of the PES. The ²Π_{1/2} spin state potential energy curve is shifted to match the spin-free potential energy curve at the maximum distances. The figure uses the same geometry and color code as Figure 4.

basis sets gives the most accurate QM energies for BrHOCO⁺, which are -741 and -731 meV, respectively. The MP2 results are best with the PP and UMP2 with cc-pVDZ/PP and cc-pVTZ/PP are ~ -740 and -730 meV, respectively, as compared to the CCSD(T)/CBS(D+T) value of -710 meV. Considering the performance of different electronic structure theory methods in reproducing the “accurate” ΔE_r^{QM} and the QM energy for BrHOCO⁺, B3LYP/aug-cc-pVDZ/lanl2dzdp and UMP2/cc-pVTZ/PP are the best QM methods for the direct dynamics simulations.

It is important to verify that B3LYP/aug-cc-pVDZ/lanl2dzdp and UMP2/cc-pVTZ/PP are able to represent the van der Waals intermediate complex [HBr...OCO]⁺. The relative energy of [HBr...OCO]⁺ from B3LYP/aug-cc-pVDZ/lanl2dzdp and UMP2/cc-pVTZ/PP are -705 and -532 meV, respectively, as compared to the CCSD(T)/CBS(D+T) value of -541 meV. B3LYP/aug-cc-pVDZ substantially overestimates this van der Waals’ interaction and only UMP2/cc-pVTZ/PP yields accurate energies for ΔE_r^{QM} , BrHOCO⁺, and [HBr...OCO]⁺.

B. Spin-orbit coupling

The ²Π_{3/2} and ²Π_{1/2} spin-orbit splitting has been measured for HBr⁺ and is 329 meV.^{12,21} For the Br atom, the measured ²P_{3/2} and ²P_{1/2} spin-orbit splitting is 456.9 meV.⁴⁷

The corresponding calculated splittings, as described in Sec. II C, are 295 meV for HBr⁺ and 411.7 meV for Br, both about 10% smaller than the experimental values. Hence, the calculated spin orbit contribution to the reaction energy is 10 meV, only 2 meV smaller than the experimental one (see Sec. II B).

The SO calculations were divided into two sets. One for the entrance-channel region of the PES from the reactants HBr⁺ + CO₂ to the reaction intermediate BrHOCO⁺, and the other for the exit-channel region from the intermediate to the products HOCO⁺ + Br. Representative potential energy scans for the entrance- and exit-channel regions of the PES are shown in Figures 3 and 4, respectively. Additional scans for the entrance-channel region are given in the supplementary material.⁵⁸ Included in each scan is the spin-free potential energy curve and the potential energy curves for the HBr⁺ ²Π_{3/2} and ²Π_{1/2} spin-orbit states. The properties of these curves are discussed in the following.

1. SO coupling for the ²Π_{3/2} HBr⁺ PES

As shown in Figures 3, 4, and S1 in the supplementary material,⁵⁸ the spin-free potential energy curves are nearly identical to those for HBr⁺ in the ²Π_{3/2} state, except the former are higher in energy. For the asymptotic HBr⁺ + CO₂ reactants, the spin-free curve is 3.49 kcal/mol higher in energy, while for the Br + HOCO⁺ asymptotic products, this difference is

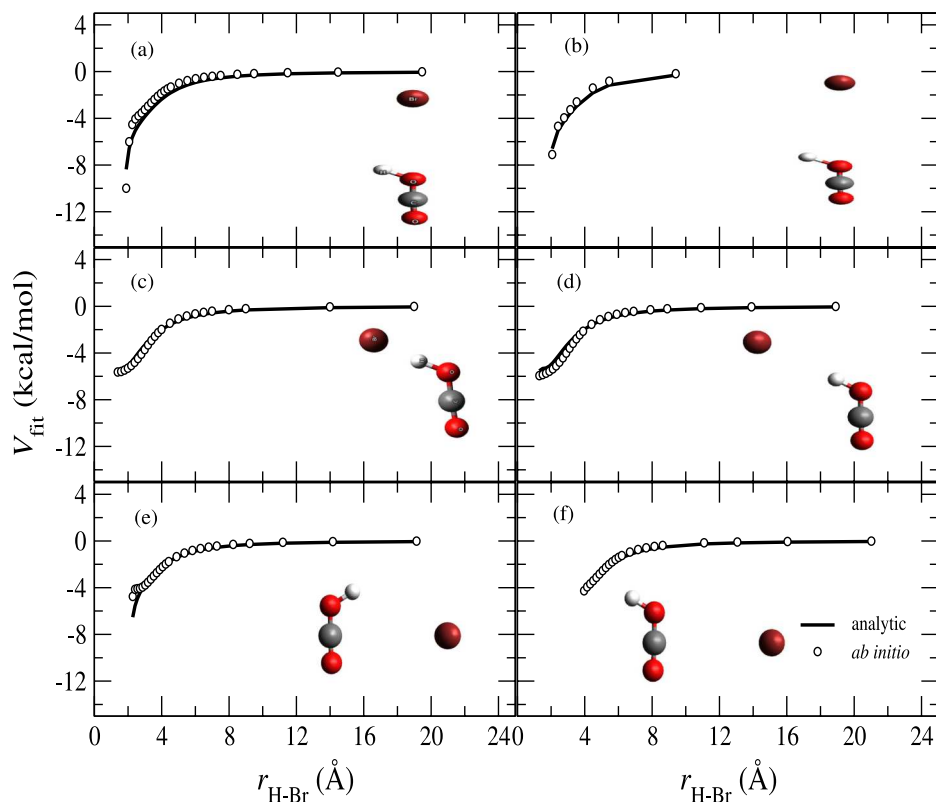


FIG. 6. V_{fit} (see Eq. (7)) is presented for six different product, exit-channel scans along with the fit to the two body potential energy form as shown in Eq. (8). The dotted points are the differences between the spin free and $^2\Pi_{1/2}$ states for those scans whereas the solid lines are the fit to those points. The order of the orientations, (a)–(f), is same as the order in Figure 5.

3.24 kcal/mol. Thus, using the spin-free PES to represent HBr^+ in the $^2\Pi_{3/2}$ state only introduces a 0.25 kcal/mol error in the relative energies of the asymptotic reactants and products.

If the spin-free and $^2\Pi_{3/2}$ potential energy curves are shifted so that their potential energies are identical at the maximum distances in the plots, e.g., 20 Å in scan (a), the resulting potential energy curves are nearly identical for the scans, as shown in Figures S2 and S3 of the supplementary material.⁵⁸ The only significant differences are for two of the entrance-channel scans in Figure 3 (the shifted curves are in Figure S2 of the supplementary material⁵⁸). For the shortest distance in scan (b), the spin-free potential energy is 4.11 kcal/mol higher than that for the $^2\Pi_{3/2}$ state; and for the repulsive region in scan (f), the spin-free curve is higher in energy. The only significant differences in the spin-free and $^2\Pi_{3/2}$ exit-channel scans in Figure 4 (the shifted curves are in Figure S3 of the supplementary material⁵⁸) are for the shortest distances in the scans (a) and (b), where the spin-free potential energies are 1.37 and 1.88 kcal/mol higher than those for the $^2\Pi_{3/2}$ state, respectively.

The only significant differences between the spin-free and $^2\Pi_{3/2}$ potential energy curves are for short-range repulsive interactions. Thus, the spin-free PES is expected to be a quite good model for both the entrance- and exit-channel regions of the PES for HBr^+ in the $^2\Pi_{3/2}$ state and may be used in direct dynamics simulations for this state.

2. SO coupling for the $^2\Pi_{1/2}\text{HBr}^+$ PES

Comparisons of scans for the spin-free potential energy and those for the $^2\Pi_{1/2}$ state are shown in Figures 3, 4, and S1 in the supplementary material.⁵⁸ For the entrance-channel scans in Figure 3, there is a very good agreement between the spin-

free and $^2\Pi_{1/2}$ state potential energy curves. For the asymptotic $\text{HBr}^+ + \text{CO}_2$ reactants, the $^2\Pi_{1/2}$ state is 3.32 kcal/mol higher than the spin-free curve. If the entrance-channel spin-free and $^2\Pi_{1/2}$ potential energy curves are shifted so that their potential energies are identical at the maximum distances in the plots, the resulting potential energy curves for the scans are nearly identical as shown in Figure S4 in the supplementary material.⁵⁸ The only significant difference is for the shortest distance in Figure 3(b) (the shifted curves are in Figure S4 of the supplementary material⁵⁸) where the $^2\Pi_{1/2}$ energy is 3.97 kcal/mol higher in energy than the spin-free value. Thus, the spin-free PES is a very good representation of that for the $^2\Pi_{1/2}$ state in the $\text{HBr}^+ + \text{CO}_2$ entrance channel, with the latter lowered by 3.32 kcal/mol.

Figure 4 shows there are important differences between the spin-free and $^2\Pi_{1/2}$ potential energy curves in the exit-channel region of the PES. At the $\text{Br} + \text{HOCO}^+$ product asymptotic limit, the $^2\Pi_{1/2}$ energy is 3.15 kcal/mol lower than the spin-free energy. Figure 5 compares the spin-free and $^2\Pi_{1/2}$ potential energy curves for the exit-channel scans, with the potential energy curves shifted so that they are identical at the scans' maximum $\text{Br} + \text{HOCO}^+$ separations. Important differences are clearly evident in the scans. In the following, an analytic function is developed to represent the effect of spin-orbit coupling for the $^2\Pi_{1/2}\text{HBr}^+ + \text{CO}_2 \rightarrow \text{Br} + \text{HOCO}^+$ reaction in the product exit-channel.

3. Analytic representation of the spin-orbit coupling for the $^2\Pi_{1/2}$ PES

A potential energy surface for the $^2\Pi_{1/2}$ state was developed by combining the spin-free potential energy surface with an analytic, i.e., MM-like, representation of the differences

between the spin-free curves and those for the ${}^2\Pi_{1/2}$ state. The function for the ${}^2\Pi_{1/2}$ PES is written as

$$V({}^2\Pi_{1/2}) = V_R S(q) + V_P [1 - S(q)], \quad (6)$$

where V_R is the PES for the reactants, entrance-channel region, V_P is the PES for the products, exit-channel region, and $S(q)$ is a switching function which connects these two regions. V_R is expressed as the $V_{spin-free} + V_R^{shift}$, where the former is the spin-free PES and the latter is the difference in the spin-free and the ${}^2\Pi_{1/2}$ potential energies when the reactants are at their asymptotic separation. V_P is expressed as

$$V_P = V_{spin-free} + V_P^{shift} + V_{fit}. \quad (7)$$

The first two terms in this equation are analogous to those for V_R , while the last is a fit to the difference between the spin-free and the ${}^2\Pi_{1/2}$ potential energy curves, with the two sets of curves shifted so that they match at the product asymptotic separation.

The differences between the shifted ${}^2\Pi_{1/2}$ and the spin-free potential energy curves, for the product, exit-channel region of the PES, are plotted in Figure 5. An accurate fit to the differences in the curves was obtained by a sum of two-body terms between the Br-atom and the H- and O-atoms of HOCO^+ . The two-body terms are written as

$$V(r) = A \exp(-Br) + C/r^n + D/r^m, \quad (8)$$

where r is the Br-H distance or one of the Br-O distances. Thus, V_{fit} was represented by a sum of the three Br-H and Br-O two-body terms. The excellent fits obtained are illustrated in Figure 6, and the fitted A , B , C , D , n , and m parameters for the Br-H and Br-O terms are listed in Table III.

The remaining component needed for the potential energy surface, $V({}^2\Pi_{1/2})$, is the switching function $S(q)$ connecting the reactant, entrance-channel and product, exit-channel regions of the potential. $S(q)$, $q = r_{H-Br} - r_{H-O}$, is given by

$$S(q) = 1.0 \quad \text{if } q \leq q_o, \quad (9)$$

$$S(q) = \exp[-a(q - q_o)^n] \quad \text{if } q > q_o,$$

where q_o , a , and n are parameters, determined by fitting Eq. (6) to all the points in the potential energy scans given in Figures 3 and 4 and the supplementary material⁵⁸ for the ${}^2\Pi_{1/2}\text{HBr}^+ + \text{CO}_2$ reaction. The resulting values for the parameters are $q_o = 0.6215 \text{ \AA}$, $a = 1263.0 \text{ \AA}^{-2}$, and $n = 2$.

TABLE III. Parameters for MM function describing spin-orbit energies for the product region of the ${}^2\Pi_{1/2}$ potential energy surface.^a

Interaction	A	B	C	D	n	m
Br-H	297.464	2.793 98	-9.565 44	-13.195 6	8	2
Br-O ₁ ^b	722.662	1.672 22	-552.752	-145.305	5	3
Br-O ₂ ^c	3298.71	18.095 0	-1515.71	-87 367.9	8	13

^aEquation (7) defines the potential energy function for the ${}^2\Pi_{1/2}$ PES. The MM fit is to Eq. (8) where units of the parameters are A in kcal/mol, B in \AA^{-1} , C in kcal $\text{\AA}^n/\text{mol}$, and D in kcal $\text{\AA}^m/\text{mol}$.

^bO₁ is the oxygen atom of HOCO^+ which is attached to the H and C atoms.

^cO₂ is the Oxygen atom of HOCO^+ which is attached only to the C atom.

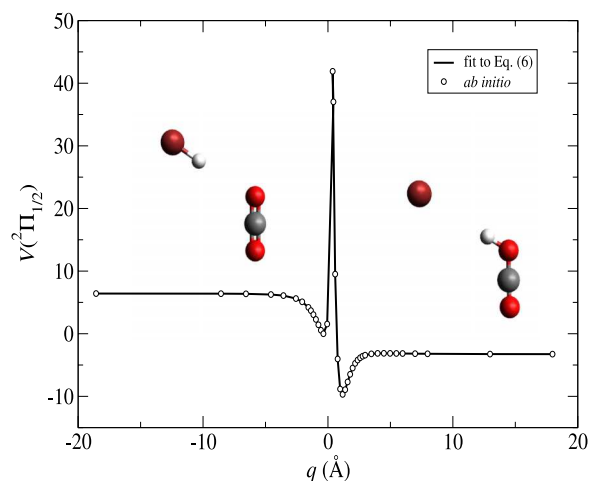


FIG. 7. Fit by the switching function of Eq. (9) to similar potential energy scans for the reactant V_R (left hand side), and the product V_P regions (right hand side) regions of $V({}^2\Pi_{1/2})$. The energy is with respect to a zero of minimum energy point of V_R . This figure is only a representation of the overall fit by Eq. (6) to all the points in the potential energy scans for $V({}^2\Pi_{1/2})$ given in Figures 3 and 4 and the supplementary material.⁵⁸

Shown in Figure 7 are illustrations of the excellent fit by this switching function to similar potential energy points for the reactant V_R and product V_P regions of the PES.

IV. SUMMARY

As described in the following, extensive calculations and analyses were made to develop accurate QM+MM PES models for the $\text{HBr}^+ + \text{CO}_2 \rightarrow \text{Br} + \text{HOCO}^+$ reaction with HBr^+ in the ${}^2\Pi_{3/2}$ and ${}^2\Pi_{1/2}$ spin-orbit states:

1. Accurate anharmonic ZPE corrections were made to obtain an accurate “experimental” energy without ZPE for the ground state $\text{HBr}^+({}^2\Pi_{3/2}) + \text{CO}_2 \rightarrow \text{HOCO}^+ + \text{Br}({}^2P_{3/2})$ reaction, to compare with the results of electronic structure calculations.
2. CCSD(T) electronic structure calculations were performed to determine “benchmark” spin-free QM energies for the $\text{HBr}^+ + \text{CO}_2 \rightarrow \text{HOCO}^+ + \text{Br}$ reaction.
3. With zero-point energies removed, the “experimental” reaction energy is $44 \pm 5 \text{ meV}$ for $\text{HBr}^+({}^2\Pi_{3/2}) + \text{CO}_2 \rightarrow \text{Br}({}^2P_{3/2}) + \text{HOCO}^+$, while the CCSD(T) value with spin-orbit effects included is 87 meV .
4. Electronic structure calculations were performed to determine structures, vibrational frequencies, and energies for the intermediates BrHOCO^+ and $[\text{HBr} \cdots \text{OCO}]^+$.
5. To determine a spin-free QM model for direct dynamics simulations, calculations were performed with a broad range of electronic structure methods and their results were compared with those obtained with CCSD(T). Only UMP2/cc-pVTZ/PP was found to be a practical and accurate QM method to use in QM+MM direct dynamics simulations.
6. The spin-free states are coupled by their SO interactions and mix, producing a new set of states ${}^2\Pi_{3/2}$ and ${}^2\Pi_{1/2}$. The SO coupling calculations were performed to determine PESs for these states.

7. The SO coupling calculations show that the spin-free QM PES gives a quite good representation of the PES for ${}^2\Pi_{3/2}\text{HBr}^+$.
8. The spin-free QM PES accurately describes the reactant, entrance-channel region of the PES for ${}^2\Pi_{1/2}\text{HBr}^+$ reaction. However, spin-orbit coupling effects are important for the product, exit-channel region of this PES. A MM model was developed to represent these effects, which were combined with the spin-free QM PES to form a QM+MM model of the PES for the ${}^2\Pi_{1/2}\text{HBr}^+$ reaction.
9. In principle, the PESs for these ${}^2\Pi_{3/2}$ and ${}^2\Pi_{1/2}\text{HBr}^+$ states are non-adiabatically coupled. However, there are no crossings of these PESs. The PESs are almost parallel in their reactant and intermediate regions and gradually approach in forming the products. Therefore, non-adiabatic transitions between the ${}^2\Pi_{3/2}$ and ${}^2\Pi_{1/2}$ states are expected to be unimportant for the $\text{HBr}^+ + \text{CO}_2 \rightarrow \text{Br} + \text{HOCO}^+$ reaction dynamics.

In future work, the PESs determined and developed here will be used in direct dynamics simulations of the $\text{HBr}^+ + \text{CO}_2 \rightarrow \text{Br} + \text{HOCO}^+$ reaction with HBr^+ in the ${}^2\Pi_{3/2}$ and ${}^2\Pi_{1/2}$ spin-orbit states.

ACKNOWLEDGMENTS

The calculations reported here are also based upon work supported by the National Science Foundation under the Partnership in International Research and Education (PIRE) Grant No. OISE-0730114, and the Robert A. Welch Foundation under Grant No. D-0005. Support was also provided by the High-Performance Computing Center (HPCC) at Texas Tech University, under the direction of Philip W. Smith. The authors thank Karl-Michael Weitzel and Lisa Paetow for very helpful suggestions.

- ¹A. A. Viggiano and R. A. Morris, *J. Phys. Chem.* **100**, 19227 (1996).
- ²S. L. Anderson, *Adv. Chem. Phys.* **82**, 177 (1992).
- ³J. Liu and S. L. Anderson, *Int. J. Mass Spectrom.* **241**, 173 (2005).
- ⁴J. Liu, B. W. Uselman, J. M. Boyle, and S. L. Anderson, *J. Chem. Phys.* **125**, 133115 (2006).
- ⁵J. M. Boyle, D. M. Bell, and S. L. Anderson, *J. Chem. Phys.* **134**, 034313 (2011).
- ⁶L. Paetow, F. Unger, W. Beichel, G. Frenking, and K.-M. Weitzel, *J. Chem. Phys.* **132**, 174305 (2010).
- ⁷L. Paetow, F. Unger, B. Beutel, and K.-M. Weitzel, *J. Chem. Phys.* **133**, 234301 (2010).
- ⁸L. Paetow and K.-M. Weitzel, private communication (2011).
- ⁹P. J. Dagdigan and M. L. Campbell, *Chem. Rev.* **87**, 1 (1987).
- ¹⁰S. G. Lias, J. E. Bartmess, J. F. Liebman, J. L. Holmes, R. D. Levin, and W. G. Mallard, *J. Phys. Chem. Ref. Data* **17**, 1 (1988).
- ¹¹P. J. Linstrom and M. G. Wallard, *NIST Chemistry Webbook*, NIST Standard Reference Database Number Vol. 69 (National Institute of Standards and Technology, Gaithersburg, MD, 2009).
- ¹²K. P. Huber and G. Herzberg, *Molecular Spectra and Molecular Structure: IV. Constants of Diatomic Molecules* (Van Nostrand Reinhold Company, New York, 1979).
- ¹³J. Liu, K. Song, W. L. Hase, and S. L. Anderson, *J. Am. Chem. Soc.* **126**, 8602 (2004).
- ¹⁴J. Liu, K. Song, W. L. Hase, and S. L. Anderson, *J. Phys. Chem. A* **109**, 11376 (2005).
- ¹⁵J. Liu and S. L. Anderson, *Phys. Chem. Chem. Phys.* **11**, 8721 (2009).
- ¹⁶J. M. Boyle, J. Liu, and S. L. Anderson, *J. Phys. Chem. A* **113**, 3911 (2009).
- ¹⁷J. Liu, K. Song, W. L. Hase, and S. L. Anderson, *J. Chem. Phys.* **119**, 2040 (2003).
- ¹⁸L. Sun and W. L. Hase, *Rev. Comput. Chem.* **19**, 79 (2003).
- ¹⁹G. Granucci and M. Persico, *J. Comput. Chem.* **32**, 2690 (2011).
- ²⁰G. Granucci and M. Persico, *Theor. Chem. Acc.* **133**, 1526 (2014).
- ²¹M. J. Haugh, B. S. Schneider, and A. L. Smith, *J. Mol. Spectrosc.* **51**, 123 (1974).
- ²²M. Valiev, E. J. Bylaska, N. Govind, K. Kowalski, T. P. Straatsma, H. J. J. van Dam, D. Wang, J. Nieplocha, E. Apra, T. L. Windus, and W. A. de Jong, *Comput. Phys. Commun.* **181**, 1477 (2010).
- ²³K. Raghavachari, G. W. Trucks, J. A. Pople, and M. Head-Gordon, *Chem. Phys. Lett.* **157**, 479 (1989).
- ²⁴A. Szalbo and N. S. Ostlund, *Modern Quantum Chemistry, Introduction to Advanced Electronic Structure Theory* (Dover, New York, 1996).
- ²⁵K. A. Peterson, *J. Chem. Phys.* **119**, 11099 (2003).
- ²⁶K. A. Peterson, D. E. Woon, and T. H. Dunning, Jr., *J. Chem. Phys.* **100**, 7410 (1994).
- ²⁷H. Hellmann, *J. Chem. Phys.* **3**, 61 (1935).
- ²⁸P. Gombas, *Z. Phys.* **94**, 473 (1935).
- ²⁹M. Krauss and W. J. Stevens, *Annu. Rev. Phys. Chem.* **35**, 357 (1984).
- ³⁰W. C. Ermler, R. B. Ross, and P. A. Christiansen, *Adv. Quantum Chem.* **19**, 139 (1988).
- ³¹M. Dolg and X. Cao, *Chem. Rev.* **112**, 403 (2012).
- ³²D. Feller, *J. Comput. Chem.* **17**, 1571 (1996).
- ³³K. L. Schuchardt, B. T. Didier, T. Elsethagen, L. Sun, V. Gurumoorthi, J. Chase, J. Li, and T. L. Windus, *J. Chem. Inf. Model.* **47**, 1045 (2007).
- ³⁴A. D. Becke, *J. Chem. Phys.* **98**, 5648 (1993).
- ³⁵C. Adamo and V. J. Barone, *Chem. Phys.* **110**, 6158 (1999).
- ³⁶H. L. Schmider and A. D. Becke, *J. Chem. Phys.* **108**, 9624 (1998).
- ³⁷C. M. Aikens, S. P. Webb, R. L. Bell, G. D. Fletcher, M. W. Schmidt, and M. S. Gordon, *Theor. Chem. Acc.* **110**, 233 (2003).
- ³⁸B. Ruscic, R. E. Pinzon, M. L. Morton, G. von Laszewski, S. Bittner, S. G. Nijssure, K. A. Amin, M. Minkoff, and A. F. Wagner, *J. Phys. Chem. A* **108**, 9979 (2004).
- ³⁹E. B. Wilson, Jr., J. C. Decius, and P. C. Cross, *Molecular Vibrations* (Dover Publications, Inc., New York, 1955).
- ⁴⁰I. N. Levine, *Molecular Spectroscopy* (John Wiley & Sons, New York, 1975).
- ⁴¹See <http://webbook.nist.gov/chemistry/> for The National Institute of Standards and Technology.
- ⁴²R. S. Grev, C. L. Janssen, and H. F. Schaefer, *J. Chem. Phys.* **95**, 5125 (1991).
- ⁴³M. L. Laury, S. E. Boesch, I. Haken, P. Sinha, R. A. Wheeler, and A. K. Wilson, *J. Comput. Chem.* **32**, 2340 (2011).
- ⁴⁴P. Sinha, S. E. Boesch, C. Gu, R. A. Wheeler, and A. K. Wilson, *J. Phys. Chem. A* **108**, 9213 (2004).
- ⁴⁵J. P. Merrick, D. Moran, and L. Radom, *J. Phys. Chem. A* **111**, 11683 (2007).
- ⁴⁶A. P. Scott and L. Radom, *J. Phys. Chem.* **100**, 16502 (1996).
- ⁴⁷A. Kramida, Y. Ralchenko, J. Reader, and NIST ASD Team, *NIST Atomic Spectra Database*, version 5.2, National Institute of Standards and Technology, Gaithersburg, MD, 2012; available online at <http://physics.nist.gov/asd>.
- ⁴⁸H.-J. Werner, P. J. Knowles, G. Knizia, F. R. Manby, and M. Schutz, *WIREs: Comput. Mol. Sci.* **2**, 242 (2012).
- ⁴⁹N. Yamamoto, T. Vreven, M. A. Robb, M. J. Frisch, and H. B. Schlegel, *Chem. Phys. Lett.* **250**, 373 (1996).
- ⁵⁰T. H. Dunning, Jr., *J. Chem. Phys.* **90**, 1007 (1989).
- ⁵¹O. Meroueh, Y. Wang, and W. L. Hase, *J. Phys. Chem. A* **106**, 9983 (2002).
- ⁵²K. Park, B. Deb, K. Song, and W. L. Hase, *J. Am. Soc. Mass Spectrom.* **20**, 939 (2009).
- ⁵³G. L. Barnes and W. L. Hase, *J. Am. Chem. Soc.* **131**, 17185 (2009).
- ⁵⁴K. A. Peterson, D. Figgen, E. Goll, H. Stoll, and M. Dolg, *J. Chem. Phys.* **119**, 11113 (2003).
- ⁵⁵J. M. L. Martin and A. Sundermann, *J. Chem. Phys.* **114**, 3408 (2001).
- ⁵⁶A. Halkier, T. Helgaker, P. Jorgensen, W. Klopper, H. Kock, J. Olsen, and A. K. Wilson, *Chem. Phys. Lett.* **286**, 243 (1998).
- ⁵⁷A. J. C. Varandas, *J. Chem. Phys.* **113**, 8880 (2000).
- ⁵⁸See supplementary material at <http://dx.doi.org/10.1063/1.4913767> for more information about spin-orbit coupling energy calculation.

Supporting Information

Figure S1. Potential energy (kcal/mol) scans with distance in Å for the $\text{HBr}^+ + \text{CO}_2$ entrance-channel region of the PES. The red, blue and black lines/dots are, respectively, for the spin-orbit free potential energy curve and the curves for the $\text{HBr}^+ \ ^2\Pi_{3/2}$ and $\ ^2\Pi_{1/2}$ states. The figure on the right are only plotting spin-orbit free potential energy curve and the curves for the $\text{HBr}^+ \ ^2\Pi_{3/2}$ states, with the $\text{HBr}^+ \ ^2\Pi_{3/2}$ states shifted so that their potential energies are identical at the maximum distances in the plots. (g) and (h): CO_2 and HBr^+ are fixed at their optimized structures, except CO_2 is bend with OCO angle to be 150° ; (i) CO_2 and HBr^+ are fixed at their optimized structures and HBr^+ is approaching CO_2 with Br closer to O, (j) same as (i), except HBr^+ is approaching from a different orientation and the distance between Br and H is enlarged to 2.1 \AA .

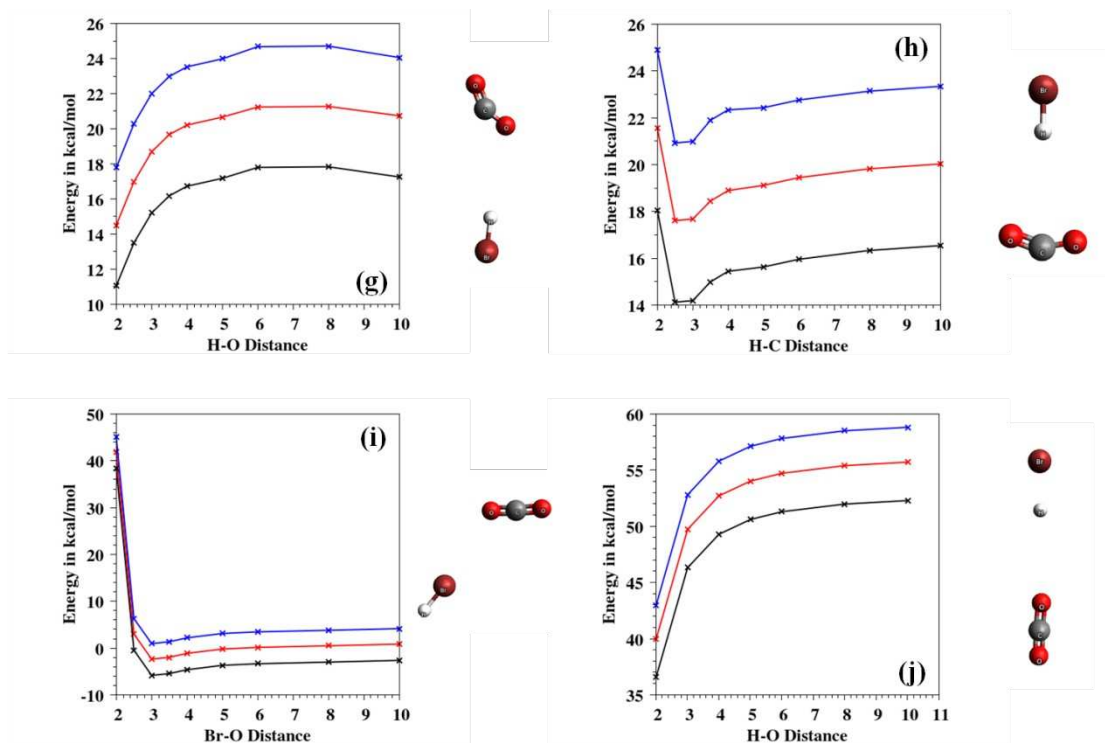


Figure S2. Potential energy (kcal/mol) scans with distance in Å for the $\text{HBr}^+ + \text{CO}_2$ entrance-channel region of the PES. The $^2\Pi_{3/2}$ spin state potential energy curve is shifted to match the spin-free potential energy curve at the maximum distances. The figure uses the same geometry and color code as Figure 3 and S1.

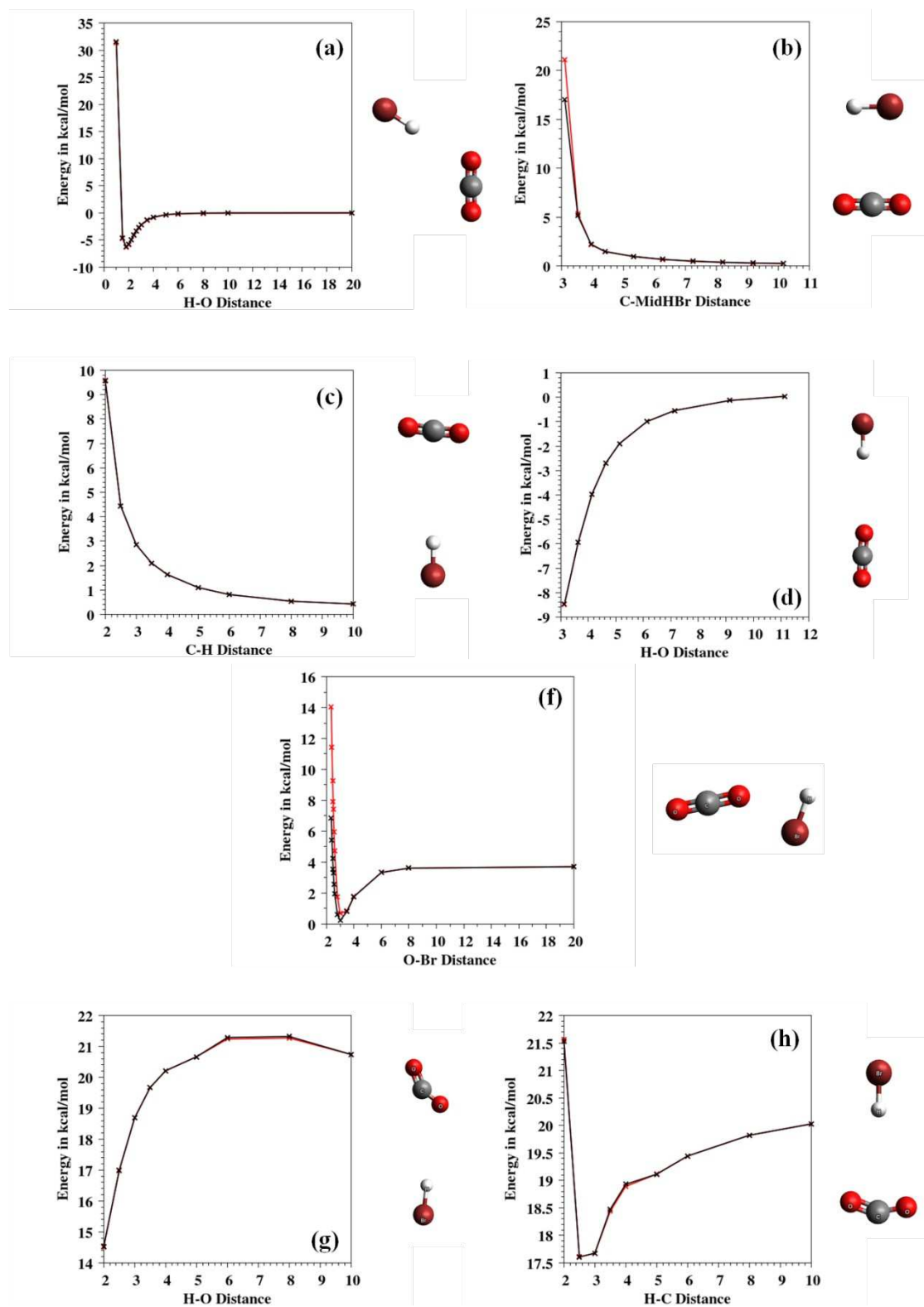


Figure S2. Count.

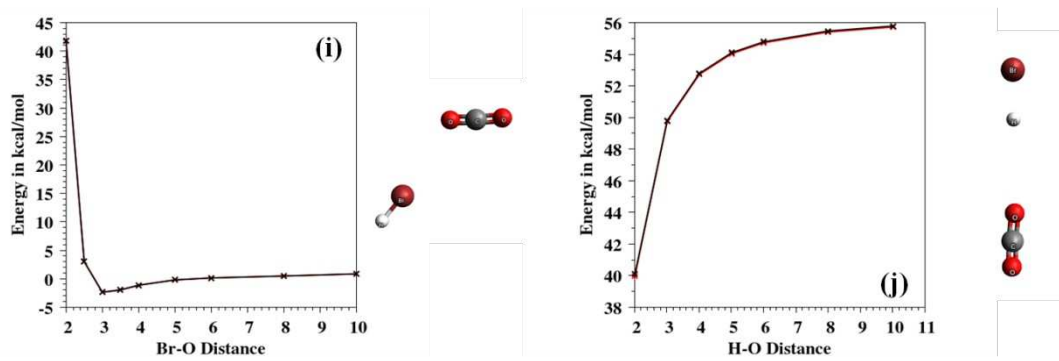


Figure S3. Potential energy (kcal/mol) scans with distance in Å for the Br + HOCO⁺ exit-channel region of the PES. The ²Π_{3/2} spin state potential energy curve is shifted to match the spin-free potential energy curve at the maximum distances. The figure uses the same geometry and color code as Figure 4.

Exit Channel Scans

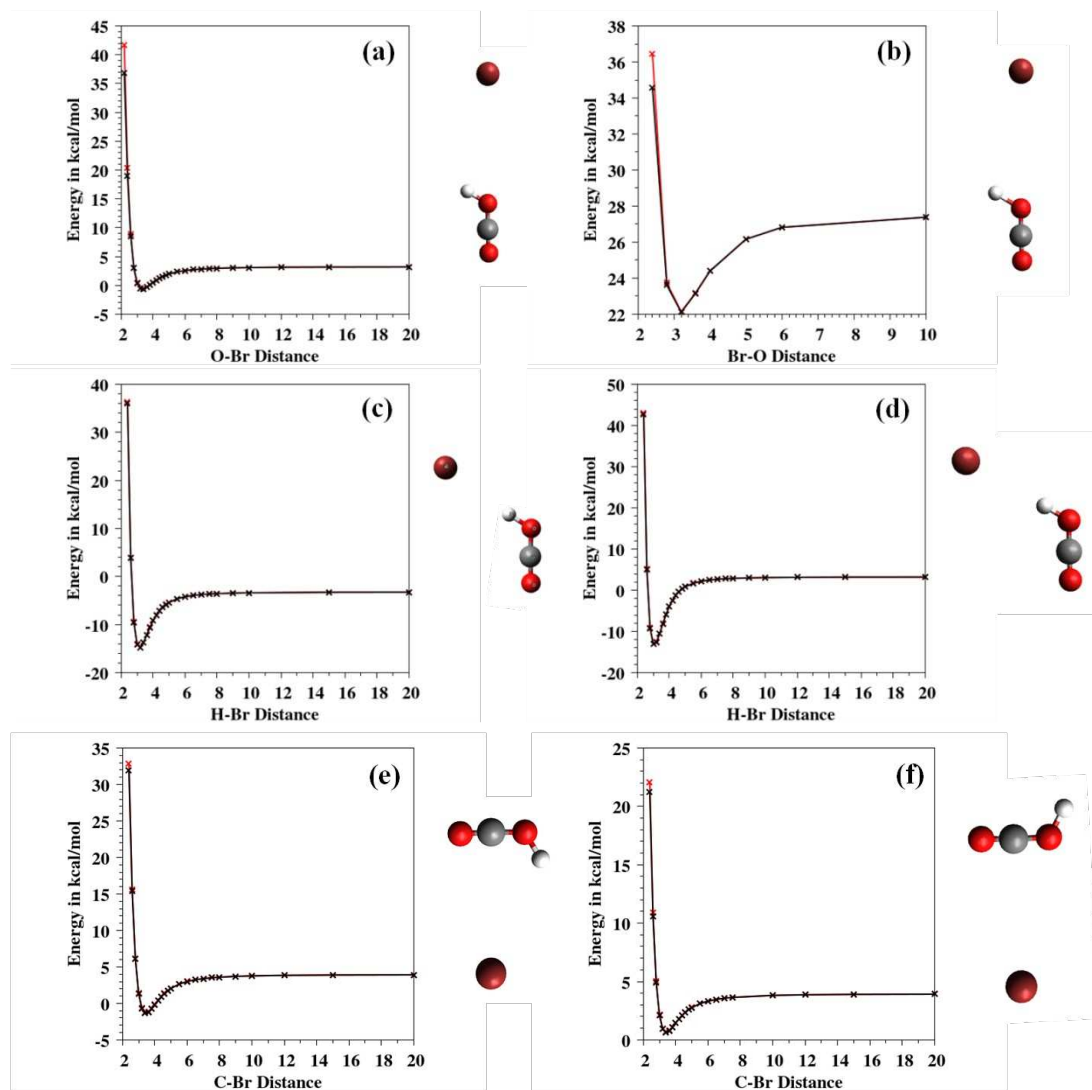


Figure S4. Potential energy (kcal/mol) scans with distance in Å for the $\text{HBr}^+ + \text{CO}_2$ entrance-channel region of the PES. The $^2\Pi_{1/2}$ spin state potential energy curve is shifted to match the spin-free potential energy curve at the maximum distances. The figure uses the same geometry and color code as Figure 3 and S1.

Entrance Channel Scans

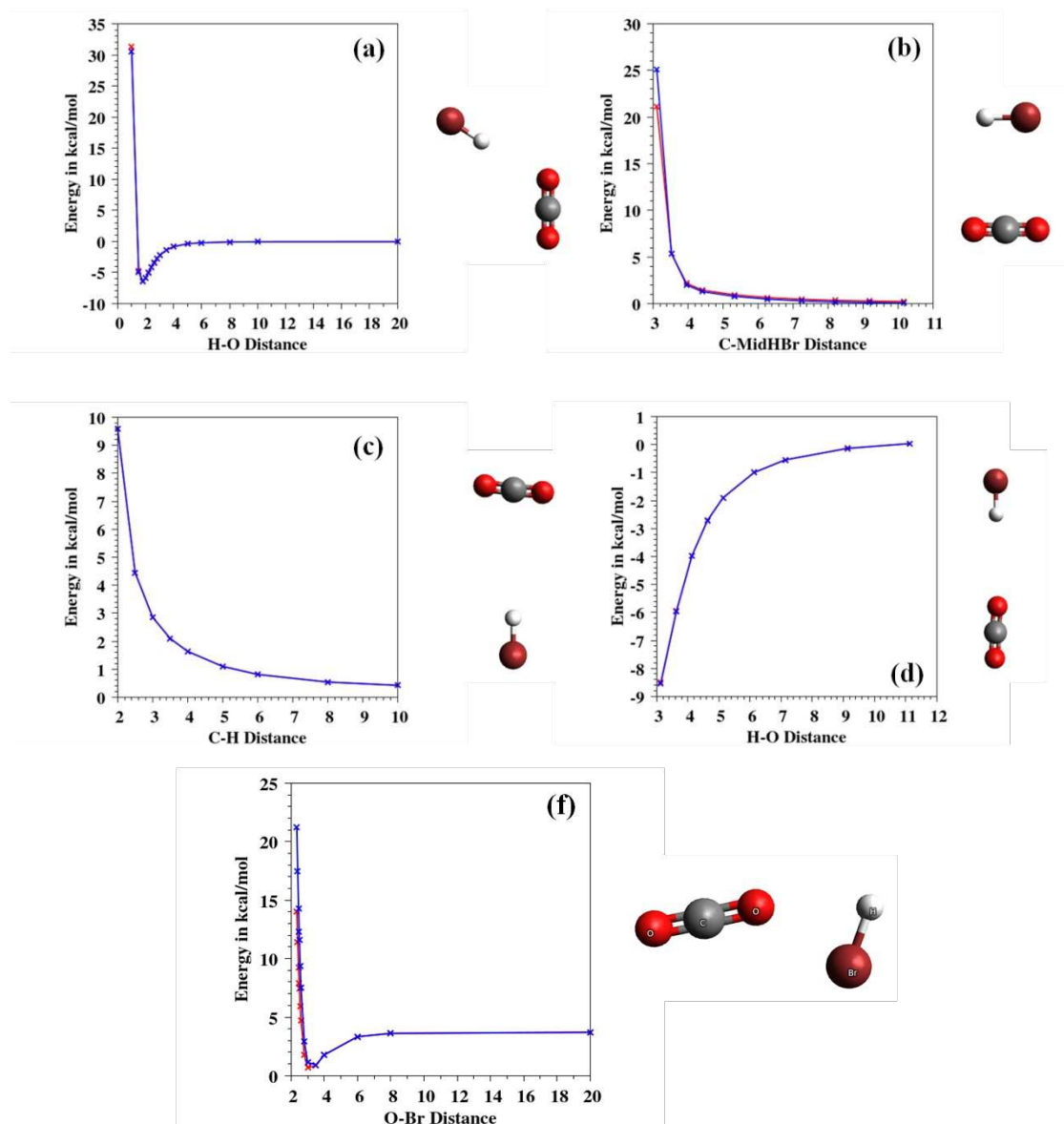


Figure S4. Count.

